Author Responses to Referees

We would like to thank both reviewers for their significant time spent reading the manuscript and for their constructive comments for improving it. We have made very careful revisions to address all these comments. In the following paragraphs, the **bolded** words represent the reviewers' original comments and the unbolded text represents our answers.

Referee 1:

In the paper titled "EVALUATION OF UV AEROSOL RETRIEVALS FROM AN OZONE LIDAR", the authors described a new approach for retrieving aerosol properties using an ozonelidar (DIAL). The use of an ozone lidar for aerosol retrievals is rather interesting yet I have some issues with the paper, listed below, that I hope the authors can address.

Several of the parameters, including the lidar ratio and aerosol backscatter color ratio, are a strong function of aerosol type. A lidar ratio of 60 is assumed with a 20% uncertainty. The aerosol backscatter color ratio is assumed to be 1.34 with an uncertainty of ±0.11. Note that for different aerosol types, both parameters could change significantly (beyond their mentioned uncertainties). It is unsure if aerosol type could be derived from the proposed method. Without a valid method for retrieving aerosol types, generalized applications of the proposed method may be problematic. The authors should at least clearly illustrate the limitations.

AERONET data are also available from the Huntsville AERONET site. I wonder if the authors could inter-compare AERONET AODs with HSRL/ RO3QET lidar derived AODs. At least the authors should compare HSRL and AERONET AODs. The retrieved aerosol profiles are used to further refine ozone retrievals. I was wondering if the refined ozone retrievals can be further used for refining aerosol retrievals.

We have accepted the reviewer's suggestion and added a paragraph on RO_3QET data evaluation using collocated AERONET data at 340 nm (Lines 213-237 in the change-tracked version). The AOD from RO_3QET and AERONET are highly correlated, with r = 0.97. The RO_3QET AOD is on average 15% larger than the AERONET AOD due to the shorter wavelength of the lidar measurement, suggesting that the choice of S = 60 sr is very reasonable. For a rough estimation, the one-sigma standard deviation (9%) of the differences can be considered as the uncertainty for S if the variability of these differences are mostly due to the variation in S. (If S has uncertainty > 9%, we expect the one-sigma value of the differences to be larger than 9% since AERONET measures extinction and RO_3QET directly measures backscatter.) Considering that AERONET measures the column average AOD, with longer temporal integration, has its own uncertainty, and covers only 38% of the total observational period, the ±20% uncertainty of S for a higher vertical resolution measurement should be large enough to cover various uncertainty sources. Therefore, the additional AERONET data not only convinces us that the data quality of both instruments is good, but also confirms that the assumed S *a priori* and uncertainty are appropriate.

We agree with the reviewer that the lidar ratio changes with aerosol type and that it is hard to derive the aerosol type from elastic lidar measurements. We have provided caveats and limitations of this work in multiple places in the text. For example, in Lines 111-113, we say: **"**The S *a priori* value assumed for this study represents a mix of urban and smoke aerosols during the lidar observations (Ackermann, 1998; Burton et al., 2012; Cattrall et al., 2005; Groß et al., 2013; Müller et al., 2007). The *a priori* is application dependent." Further, in Lines 326-329 in the Conclusions section, we say: "These exponents represent a summertime average for a mixture of urban pollution and fire smoke. Speciation of aerosol types was not done in this work, although we recognize that S and Ångström exponent vary with the aerosol phase function and size distribution.**"**

1. **Other comments Line 121, "as you go towards the" -who is "you"?**

To address this issue, we have changed “decreases as you go towards the ground from the far range” to “decreases towards the ground from the far range”.

2. **Line 141, “10-min temporal average and 30-m spatial average for both HSRL”. -Should be “30-m vertical average”?**

We have replaced “spatial” with “vertical” as per suggestion.

3. **Lines 151-152, “Therefore, data contaminated by clouds is filtered out. ”-What are the cloud screening steps? Those steps need to be included.**

The cloud screening process is described at Line 89-95 in Section 2.1. We have added additional description to clarify our cloud treatment: “The cloud base height is determined by the following empirical method. Derivatives of the logarithm of the off-line analog signal are calculated for a lidar signal profile and the first range bin at which the derivative is greater than a certain threshold is considered to be the cloud base height. The threshold is chosen empirically based on the lidar SNR and the vertical resolution. Lidar data with cloud base lower than 2 km was discarded.”

4. **Lines 170-171, “The slope of the regression (2.16) results in the best” -what is “(2.16)” referring to?**

To clarify, we change this sentence to “the slope of the regression, equal to 2.16, results in …”.

5. **Line 278, equation A2, need a reference for this equation.**

We have added (Uchino et al., 1980) as the reference for Equation (A2).

6. **Line 306, equation B1, need a reference for this equation. Equations B3 and B4. Define ΔβsigA(r) and δβsigA(r).**

We have added (Taylor, 1997) as the reference for Equation (B1) a Line 374.

At Line 374, we made a change to reflect the definition of $\Delta\beta^{sig}_{A}(r)$ as: “…we obtain the uncertainty of the aerosol backscatter owing to lidar signal measurement error, $\Delta\beta^{sig}_{A}(r)$, relative to the total backscatter as…”.

The definition of $\delta\beta^{sig}_{A}(r)$ is already stated at Line 387 ahead of Equation (B3), so there is no change for that.

Referee 2:

1 General Remarks

The authors give a comprehensive description of their approach for retrieving aerosol backscatter profiles from the return signals of an atmospheric lidar operating in the UV near 290 nm. Their aerosol results in the UV are compared with HSRL lidar measurements of aerosol at 532 nm. Generally good agreement is found. Uncertainties of the retrieved aerosol properties in the UV are also estimated. They usually exceed 50% over a wide range of altitudes.

I agree with reviewer 1 that comparison to Aeronet optical depth data would be a good addition to the paper. I also agree with reviewer 1 that a few more cautionary remarks on the variation of extinction to backscatter ratio and aerosol wavelength dependences between aerosol types should be added. However, in many cases the stated large uncertainties probably cover a good fraction of these changes between aerosol types.

Overall I think this is a solid paper, well suited to the scope of AMT. I recommend publication with only a few minor revisions.

We thank the reviewer for the positive comments and good suggestions. We have added a paragraph on RO_3QET data evaluation using collocated AERONET data at 340 nm (Lines 213-237) to address both reviewers' suggestion. The AERONET data provide a very nice evaluation of the ozone lidar data and the assumed lidar ratio. (Please refer to the answers to Reviewer 1 for more details.) The references for AERONET have been also added.

2 Suggestions

1. **line 33: "weighing" or "weighting"?**

We meant "weighing", so we keep it unchanged.

2. **lines 35/36: I suggest to add the Browell et al. 1985 reference here as well. Ed Browell really pioneered operational airborne UV-lidar measurements of tropospheric ozone in the 1980s.**

We agree and we have added Browell et al. 1985 in the citation list here.

3. **lines 32 to 42: Here, and in several other places of the paper (e.g. lines 256 to 262), I suggest to add more cautionary sentences on the general problem of aerosol interference on DIAL ozone measurements (Browell et al. 1985, but also Steinbrecht and Carswell, JGR, 1994). Especially the differential backscatter term can cause large problems for narrow aerosol layers (errors exceeding 10s of percents). Investigations of aerosol effects on ozone, of the order of a few percent, are very desirable, but substantial caution is required.**

We have cited Steinbrecht and Carswell (1994) in the 1st paragraph.

4. **lines 48/49: there is ozone absorption at 532 nm, which is not necessarily negligible. Add statement.**

We have replaced "negligible" with "much smaller than".

5. **lines 55 to 62: Maybe the authors should move this to the beginning of the paragraph, and even extend it? Important lidar facts are: Because of the strong wavelength dependence of molecular Rayleigh scattering (λ^{-4}), and the weaker wavelength dependence of aerosol scattering ~$\lambda^{-1.5}$, aerosol is measured best by lidars at 532 and 1064 nm (NdYAG) or 694 nm (Ruby). Nevertheless, the authors' UV lidar also measures aerosol, and aerosol interference on the ozone measurement needs to be looked at. Fortunately, because of the large increase of ozone extinction from 320 nm to 250 nm (2 orders of magnitude), aerosol interference at your wavelengths (around 290 nm) is a factor of 5 to 20 smaller than, e.g., for a stratospheric ozone DIAL (around 310 nm) for the same amount of aerosol.**

We have made change to say: "Lasers used for aerosol lidars are preferred in the visible and infrared bands, typically 532 and 1064 nm for Nd:YAG laser or 694 nm for Ruby laser (Russell et al., 1979),…".

We agree with the reviewer on the aerosol interference in the ozone DIAL retrieval approximately proportional to $\Delta\lambda/(\lambda\Delta\alpha_{O3})$. The aerosol interference in DIAL is pretty complicated and is worth another paper to discuss. Since the major purpose of this article is to discuss aerosol retrieval and its uncertainty, we decide not to add more discussion on the aerosol interference in DIAL retrieval. But, this is certainly an important motivation to do aerosol retrieval. So, in the Introduction, we say "Vertical aerosol profiles are of high interest not only because they are needed for aerosol correction in ozone lidar retrievals (Steinbrecht and Carswell, 1994), …". In the Conclusions, we write "Aerosol correction for ozone lidar retrievals will be described in a subsequent paper."

6. **line 154: "owning" -> "owing"?**

We have made the correction as per the suggestion.

7. **line 186: Why is the extinction wavelength exponent (1.49) different from the backscatter wavelength exponent (1.34). Is that because the constant lidar ratio (S = 55) is only used for the UV lidar, whereas the HSRL actually measures extinction? The authors might want to clarify that. I also wonder how meaningful this entire extinction comparison then is, because the UV lidar really only measures backscatter, and extinction is largely assumed.**

Yes. The extinction wavelength exponent is different from the backscatter exponent because the lidar ratio (*S*) is wavelength dependent. After an extensive literature review, we assumed S=60 sr at 299 nm and the resulting extinction retrievals agree well with the AERONET observations at 340 nm (we have added this description in the AERONET-DIAL comparison). The *S*=55 sr assumption for the HSRL at 532 nm is taken from Reid et al. 2017, who derived this value by comparing HSRL data (532 nm) with collocated AERONET observations at 500 nm. To clarify this, we have added "the calculated Ångström exponent is different from the backscatter-related wavelength exponent because of the wavelength dependence of *S*."

Yes, as the reviewer pointed out, the elastic lidar directly measures backscatter so that the extinction retrieval has larger uncertainty than backscatter retrieval. However, we still believe the extinction retrieval is meaningful because "In practice, aerosol extinction is a more meaningful parameter and more relevant for several applications than backscatter" (Lines 203), such as AOD calculations to compare with satellite data.

8. **lines 225 to 236: In Fig. 2, the UV lidar measured backscatter above 6 km during daytime clearly is too high (lighter blue colors). The authors state that they are not looking at these altitudes. However, I am wondering if the systematic high bias above 5 km in Fig. 4, has something to with the daytime high bias above 6 km in Fig. 2? Have the authors considered that? A few additional sentences might be good.**

We agree that the large positive differences above 5 km can be due to strong solar background during daytime. We have added the following explanation:

"These positive biases can be caused by two reasons. First, the RO_3QET derived aerosol extinction above 5 km is obviously larger than that from HSRL during daytime due to the solar background impact, which is especially strong in the summer. The relative differences are even worse in clean (compared to turbid) regiosn during the daytime because of the small number division effect mentioned earlier. It can be seen from Figure 3 that RO_3QET nighttime retrievals above 5 km and daytime retrievals below 5 km are relatively good due to either lower solar background or larger lidar signal resulting in better SNR."

9. **Figure 3: Maybe a logarithmic plot (both axes) would be better here? A lot of the data points are close to the lower left corner (0,0).**

We have accepted the reviewer's suggestion and changed the linear scale to log scale for Figure 3 (currently Figure 4). There are about 80,000 points in that figure, with a large number being very small values. So, the log scale is better to show how the points are scattered relative to the regression line.

EVALUATION OF UV AEROSOL RETRIEVALS FROM AN OZONE LIDAR

Shi Kuang[1]*, Bo Wang[1], Michael J. Newchurch[1], Kevin Knupp[1], Paula Tucker[1], Edwin W. Eloranta[2], Joseph P. Garcia[2], Ilya Razenkov[2], John T. Sullivan[3], Timothy A. Berkoff[4], Guillaume Gronoff[4,5], Liqiao Lei[4,6], Christoph J. Senff[7,8], Andrew O. Langford[7], Thierry Leblanc[9], Vijay Natraj[10]

[1]University of Alabama in Huntsville, Huntsville, Alabama, USA
[2]University of Wisconsin-Madison, Madison, Wisconsin, USA
[3]NASA Goddard Space Flight Center, Greenbelt, Maryland, USA
[4]NASA Langley Research Center, Hampton, Virginia, USA
[5]Science Systems and Applications Inc., Lanham, Maryland, USA
[6]Universities Space Research Association, Columbia, Maryland, USA
[7]NOAA Earth System Research Laboratory, Boulder, Colorado, USA
[8]Cooperative Institute for Research in Environmental Sciences, University of Colorado, Boulder, Colorado, USA
[9]Jet Propulsion Laboratory, California Institute of Technology, Wrightwood, CA, USA
[10]Jet Propulsion Laboratory, California Institute of Technology, Pasadena, California, USA

*_Correspondence to_: Shi Kuang (kuang@nsstc.uah.edu)

Abstract

Aerosol retrieval using ozone lidars in the ultraviolet ~~(UV) band~~spectral region is challenging but necessary for correcting aerosol interference in ozone retrieval and for studying the ozone-aerosol correlations. This study describes the aerosol retrieval algorithm for a tropospheric ozone lidar, quantifies the retrieval error budget, and intercompares the aerosol retrieval products at 299 nm with those at 532 nm from a high spectral resolution lidar (HSRL) and with those at 340 nm from an Aerosol Robotic Network radiometer. After the cloud-contaminated data is filtered out, the aerosol backscatter or extinction coefficients at a 30-m and 10-min resolution retrieved by the ozone lidar are highly correlated with the HSRL products, with a coefficient of 0.95 suggesting that the ozone lidar can reliably measure aerosol structures with high spatio-temporal resolution when the signal-to-noise ratio is sufficient. The actual uncertainties of the aerosol retrieval from the ozone lidar generally agree with our theoretical analysis. The backscatter color ratio (backscatter-related exponent of wavelength dependence) linking the coincident data measured by the two instruments at 299 and 532 nm is 1.34±0.11 while the Ångström (extinction-related) exponent is 1.49±0.16 for a mixture of urban and fire smoke aerosols within the troposphere above Huntsville, AL, USA.

1. Introduction

A tropospheric ozone differential absorption lidar (DIAL) makes measurements of vertical ozone profiles, typically at two wavelengths chosen between 277 and 300 nm with a separation less than 12 nm, by weighing several parameters such as the ozone absorption cross sections, solar background, dynamic range of the detection system, and interference from aerosols and other species (e.g., Alvarez et al., 2011; Browell et al., 1985; De Young et al., 2017; Fukuchi et al.,

Formatted: Superscript

2001; Kempfer et al., 1994; McDermid et al., 2002; Proffitt and Langford, 1997; Strawbridge et al., 2018; Sullivan et al., 2014). Vertical aerosol profiles are of high interest not only because they are needed for aerosol correction in ozone lidar retrievals (Steinbrecht and Carswell, 1994), but also because simultaneous ozone and aerosol vertical profile measurements provide unique information on their interactions and on sources of pollutant transport (Browell et al., 1994; Langford et al., 2020; Newell et al., 1999). However, there is currently no consensus on the reliability of the aerosol retrievals produced by ozone lidars due to the difficulty of solving the three-component lidar equation and the large variability in aerosol optical properties associated with the multiplicity of aerosol types and size distributions.

The most widely used solution for the elastic single-wavelength aerosol lidar equation is the analytic method developed by Klett (1981). The inversion method then inspired Fernald (1984) to publish a computer algorithm scheme to solve the more general two-component (aerosol and molecular) atmospheric lidar equation. The Klett (1981) inversion requires *a priori* for the lidar ratio (i.e., aerosol extinction-to-backscatter ratio, represented by "*S*" thereafter) to link the aerosol backscatter with its extinction for solving the lidar equation. Lasers used for aerosol lidars are preferred in the visible and infrared bands, typically 532 and 1064 nm for Nd:YAG laser or 694 nm for Ruby laser (Russell et al., 1979), where the ozone absorption is much smaller than molecular and Mie scattering. In the ultraviolet (UV) band for an ozone lidar, the ozone absorption may not be trivial. Some ozone lidars have an aerosol channel available, either independently or sharing receiving optics with the ozone channel (e.g., Browell et al., 1994; De Young et al., 2017; Gronoff et al., 2019; Kovalev and McElroy, 1994; Uchino and Tabata, 1991). For most of the traditional two-wavelength ozone lidars without an aerosol channel, although there has been some discussion about the aerosol retrieval algorithm (e.g., Eisele and Trickl, 2005; Langford et al., 2019; Papayannis et al., 1999; Sullivan et al., 2014), the evaluation of the aerosol retrieval product and its error budget have rarely been addressed. Due to a significant wavelength difference with aerosol lidars, several aspects of the aerosol retrieval using an ozone lidar are worth noting. Firstly, the signal-to-noise ratio (SNR) for ozone lidars decays quicker with altitude due to more significant UV molecular (i.e., Rayleigh) scattering and ozone absorption resulting in a lower retrievable altitude than aerosol lidars. Secondly, since the molecular and ozone components become more important at UV wavelengths compared to visible and infrared wavelengths, the uncertainties in aerosol retrieval propagated from the calculation of these two components are expected to be larger for ozone lidars than for aerosol lidars. Thirdly, *S* and the wavelength dependence used for the ozone lidar wavelengths may be different from those used for the longer aerosol lidar wavelengths (Ackermann 1998; Eck et al., 1999).

The primary objectives of this article are to investigate the performance of our aerosol retrieval algorithm and to quantify its error budget for the ozone lidar. The secondary goal is to seek the overall wavelength dependence between the aerosol optical properties measured by the ozone lidar at 299 nm and by a high spectral resolution lidar (HSRL) at 532 nm.

2. Instruments and Data Processing

2.1. Ozone Lidar

The Rocket-city Ozone (O_3) Quality Evaluation in the Troposphere (RO_3QET) lidar is located on the campus of the University of Alabama in Huntsville (UAH) at 34.725 °N and 86.645 °W at 206 m asl and is one of the six systems of

the Tropospheric Ozone Lidar Network (TOLNet) (http://www-air.larc.nasa.gov/missions/TOLNet). This system measures ozone from 0.1 km up to about 12 km during nighttime and up to about 6 km during daytime with a temporal resolution of 2 min. The vertical resolution of the lidar retrievals varies from 150 m in the lower troposphere to 750 m in the upper troposphere in order to keep the measurement uncertainty within ±10% (Kuang et al., 2013).

The transmitter comprises two Raman-shifted lasers at 289 and 299 nm. Two 30-Hz, 266-nm Nd:YAG lasers pump two 1.8-m Raman cells, respectively, with mixtures of active gas and buffer gas to generate 289 and 299-nm lasers with an average pulse energy of about 5 mJ. The receiving system consists of three receivers with diameters of 2.5 cm, 10 cm, and 40 cm, respectively, and four photomultipliers (PMTs) similar to that described by Kuang et al. (2013) except that the solar filters have been replaced by 300-nm short-pass filters for all telescopes. Channels ~~–~~1, 2, 3, 4 represent the 2.5-cm, 10% of the 10-cm, 90% of the 10-cm, and the 40-cm telescope channels, respectively. Since the modification of Channel ~~–~~4 through the addition of narrow-band solar filters was not completed before the time period of this study, data from this channel was not used in this work, ~~resulting in~~with the net result that ~~the~~ uncertainties for ozone retrievals above 6 km during daytime were often too large due to the strong solar background. Lidar signal counting was accomplished by four Licel transient recorders (Licel company, Germany) with both analog and photoncounting (PC) modes, with a sampling rate of 40 MHz corresponding to a 3.75-m fundamental resolution. The cloud base height is determined by the following empirical method. Derivatives of the logarithm of the off-line analog signal are calculated for a lidar signal profile and the first range bin at which the derivative is greater than a certain threshold is considered to be the cloud base height. The threshold is chosen empirically based on the lidar SNR and the vertical resolution. ~~serve to label clouds by setting an appropriate threshold. The cloud filtering process should be conducted carefully because an elastic lidar without a polarization channel is not capable of accurately distinguishing aerosols and clouds solely by their backscatter properties.~~ Therefore, ~~the~~ lidar data with cloud~~s~~ base lower than 2 km was discarded. The cloud filtering process should be conducted carefully because an elastic lidar without a polarization channel is not capable of accurately distinguishing aerosols and clouds solely ~~by~~through their backscatter properties. Five 2-min lidar data intervals were combined to give a 10-min lidar-signal integration time to improve the SNR. Further, six of the 3.75-m fundamental bins were integrated for all channels. In addition, dead-time correction (for PC signal only), background correction, analog-PC signal merging, and signal-induced noise correction were performed.

2.2. ~~Introduction of the~~ Aerosol Retrieval ~~Algorithm~~ and Uncertainty Estimation

The aerosol profiles were retrieved with an iterative DIAL algorithm. A brief description of this algorithm is provided in this section, with further details in Appendix A. A first-order Savitzky-Golay differentiation filter with a second-degree polynomial was applied to the logarithm of the signal ratios to compute the first-cut ozone profile. This initial ozone profile was substituted back into the three-component lidar equation to derive the profile of aerosol backscatter coefficients at 299 nm by assuming a constant S of 60 sr and boundary value of the aerosol backscatter coefficient at a far-range reference altitude, about 10 km. During the daytime, the ozone retrieval was limited by the lower SNR of the 289-nm channel, but the 299-nm channel had much better SNR due to lower atmospheric extinction and was able to measure aerosol up to higher altitudes. S has large variability as a function of~~is highly variable with~~ aerosol characteristics, humidity, and wavelength (Ackermann, 1998; Strawbridge et al., 2018; Mishchenko et al.,

1997). The *S a priori* value assumed for this study represents a mix of urban and smoke aerosols during the lidar observations (Ackermann, 1998; Burton et al., 2012; Cattrall et al., 2005; Groß et al., 2013; Müller et al., 2007). The *a priori* is application dependent. In the aerosol retrieval uncertainty discussion in Appendix B, we assume a ±20% uncertainty for *S* based on an average standard deviation obtained from prior observations (Müller et al., 2007).

Molecular backscatter and extinction profiles were computed from local radiosonde data. Then, the aerosol profile was substituted into the lidar equation again to obtain a stable solution, usually within three iterations. This aerosol profile was further employed to calculate the aerosol correction for ozone retrievals using the first-order Taylor approximation (Browell et al., 1985) by assuming a power law wavelength dependence for the aerosol extinction and choosing an appropriate Ångström exponent. Since this ~~paper~~ work focuses only on aerosol retrieval, details of the ozone correction will be described in a future article. Finally, the aerosol profiles derived by the three altitude channels were merged into a single profile in the overlapping altitude zones, i.e., 0.5–1 km for Channels ~~–~~1 and 2 and 1.5–2 km for Channels ~~–~~2 and 3.

The primary uncertainty sources for the aerosol lidar retrievals are the uncertainties in lidar signal measurement, boundary value assumption for aerosol backscatter coefficient, air density measurement, *S a priori*, and ozone profile input. The relative importance of these sources ~~are~~ is altitude dependent. In the planetary boundary layer (PBL) where the air is typically turbid, the *S* uncertainty is dominant while other sources are minor (only few percent). The uncertainty of *S* influences the uncertainty of the aerosol backscatter through a complicated relationship. However, the magnitude of the above two uncertainties can be approximately seen to be close. At the far range (higher than 7 km), lidar signal detection noise and inaccurate boundary value assumption are important. Influence from both of the above sources, especially the boundary value, on the aerosol retrieval quickly decreases ~~as you go~~ towards the ground from the far range. In the middle range (PBL top – 7 km), both the air density measurement error and lidar signal detection noise are essential. Uncertainty due to ozone profile input is relatively unimportant and is only few percent at most altitudes. Figure B1 presents an example of the aerosol backscatter uncertainty calculated from 10-min nighttime RO_3QET lidar data. The error budget estimate generally justifies the choice of using 6 km as the maximum altitude for RO_3QET-HSRL comparison since the total uncertainty for the RO_3QET aerosol retrieval could be unacceptably large (i.e., persistently larger than 100%).

2.3. HSRL

The University of Wisconsin HSRL (Eloranta, 2005) was deployed in Huntsville, AL from 19 June to 4 November 2013 and operated almost 24 hours every day to support the Studies of Emissions and Atmospheric Composition, Clouds and Climate Coupling by Regional Surveys SEAC^{4}RS campaign (Kuang et al., 2017). The HSRL transmitter was a diode-pumped Nd:YAG laser at 532 nm with a pulse energy of about 50 μJ and a pulse repetition frequency of 4 kHz. The expanded laser beam was transmitted coaxially with a 40-cm telescope with a tiny field of view (FOV) of 100 μrad to reduce solar background. The HSRL spectral filtering can separate the molecular backscatter from the aerosol backscatter due to the molecular Doppler broadening effect while the particulate backscatter remains spectrally unbroadened. Aerosol backscatter coefficients can then be calculated as the difference between the total return and the molecular component (Grund and Eloranta, 1991). In principle, aerosol extinction can also be computed by comparing the measured attenuated molecular backscatter to a reference, unattenuated molecular backscatter profile

that is calculated from radiosonde-measured air density profile or a numerical model (Hair et al., 2008). However, small and fast signal fluctuations were found in the partial overlap region (between the surface and about 4.5 km) for the data taken in Huntsville so that aerosol extinction below 4.5 km cannot be derived with a satisfying precision. The signal fluctuations were probably caused by small optical misalignments from temperature changes within the lidar system (Reid, et al., 2017). The aerosol backscatter calculation is not affected by the lidar signal fluctuations since any range-dependent instrument effects are canceled out. Therefore, we focus on the aerosol backscatter intercomparison between the HSRL and RO_3QET. If aerosol extinction is needed for the HSRL, we will calculate it from the aerosol backscatter by assuming a constant lidar ratio. ~~We intercompare the backscatter coefficients measured by the two instruments to avoid the extra uncertainty due to the *S* assumption for the HSRL.~~ The HSRL provides aerosol products with a 30-m vertical resolution and 1-min temporal resolution from near the surface to 15 km. To achieve sufficient SNR for both HSRL and ozone lidar and to reduce the uncertainty arising from the clock bias of the controlling computers, we adopt 10-min temporal average and 30-m ~~spatial~~ vertical average for both HSRL and ozone lidar in the intercomparison study. The HSRL has a backscatter measurement precision better than 10^{-7} $(m\ sr)^{-1}$ for a 1-min signal average (Reid et al., 2017), which represents an estimated precision for the extinction coefficient of better than 2×10^{-6} m^{-1} for a 10-min average.

3. Intercomparison Results

We select four time periods (21–23 June, 14–15 August, 27–28 August, and 5–6 September, 2013) to investigate the ozone lidar capability for measuring aerosol column and range-resolved profiles. All four cases have coincident ozone lidar and HSRL observation periods longer than 24 hours, fully covering the convective mixing layer development and collapse processes (Klein et al., 2019) and having significant smoke layers in the free troposphere. Due to the significant extinction and potential multiple scattering caused by clouds, the ozone lidar is incapable of measuring either ozone or aerosol accurately above clouds, especially thick clouds. Therefore, data contaminated by clouds is filtered out. At this time, the narrow-band interference filters had not been incorporated into the receiving system and the wide-band filter resulted in substantial solar background during the daytime; hence, we set 6 km asl as the maximum altitude for intercomparison. The uncertainty of the aerosol retrieval owning to lidar signal measurement error is dominant at far range and is determined by the lidar SNR, as shown in Appendix B.2. The solar background is an important noise resulting in the lidar signal measurement error during daytime and is partly responsible for the high aerosol retrieval uncertainty above 6 km as shown by the example in Figure B1. The 10-min HSRL profiles are interpolated to the times of the ozone lidar data.

First, we investigate the correlation of the integrated (or column) aerosol backscatter between the ozone lidar and HSRL to obtain a general relationship between their averages. Figure 1 shows that the RO_3QET- and HSRL-derived integrated backscatter coefficients for all four cases are highly correlated, with a Pearson correlation coefficient of 0.99. The root mean square error (RMSE), the standard deviation of the residuals, is negligibly small at 1×10^{-3} sr^{-1}, suggesting that the linear regression equation can accurately represent the relationship between the AOD measured by the two instruments. The 493 sampling profiles cover 82 hours of coincident ozone lidar and HSRL observations. We define the aerosol backscatter color ratio ($å_\beta$) as (Burton et al., 2012):

Formatted: Superscript

Formatted: Superscript

$$å_\beta = -\frac{d(ln\beta_A)}{d(ln\lambda)} = -\frac{\ln(\frac{\beta_A^{299}}{\beta_A^{532}})}{\ln(\frac{299}{532})}, \quad (1)$$

where β_A^{299} and β_A^{532} represent the aerosol backscatter coefficient at 299 and 532 nm, respectively. The subscript "*A*" represents the "aerosol" component, to be distinguished ~~with~~ from the "molecular" contribution ~~which~~ that is represented by subscript "*M*" in the Appendix. ~~–~~$å_\beta$ is an exponent denoting backscatter-related wavelength dependence, to be distinguished from the commonly-used Ångström exponent (Ångström, 1929) that refers to the wavelength dependence of optical thickness or extinction coefficient. $å_\beta$ is also different from another often-used concept, "color ratio of the lidar ratios", which refers to the ratio of *S* at two different wavelengths. The slope of the regression, ~~(~~equal to 2.16~~,)~~ results in the best least-squares fit value of 1.34 for $å_\beta$ at 299 and 532 nm. The uncertainty of the column β_A^{299} is expected to be smaller than the uncertainty for β_A^{299} at a particular altitude and for a 10-min integration time (in Figure B1) since the average over longer time and altitude range greatly reduces the random noise as suggested by the small RMSE in Figure 1. If the uncertainty of the column β_A^{299} measurements is estimated to be 20% which is primarily due to the uncertainty of the *S a priori* (a systematic error), we can estimate the corresponding uncertainty for $å_\beta$=1.34 to be ±0.11 by error propagation from Eq. (1). $å_\beta$ has important applications in aerosol type classification from (spectral) aerosol lidar measurements (e.g., Cattrall et al., 2005; Hair et al., 2008; Müller et al., 2007). There is significant variation in $å_\beta$ for 532–1064 nm reported in different studies, with numbers ranging from negative values to 2.3 (Burton et al., 2012; Cattrall et al., 2005; Müller et al., 2007). However, all of these studies show a larger value of $å_\beta$ for smoke and urban aerosols ~~was larger~~ than for maritime and dust aerosols. Since most previous studies report $å_\beta$ ~~–~~for wavelengths longer than 355 nm, $å_\beta$ calculated in this study for 299–532 nm could provide valuable data for UV wavelengths.

In practice, aerosol extinction is a more meaningful parameter and more relevant for several applications than backscatter. For the HSRL, the extinction coefficients are linearly converted from the backscatter coefficients by assuming a constant *S* = 55 sr with 20% uncertainty, in the same manner as Reid et al. (2017). The estimated Ångström exponent for 299 and 532 nm is 1.49±0.16, using the data in Figure 1 after considering uncertainties in *S* for both lidars. The calculated Ångström exponent is different from the backscatter-related wavelength exponent because of the wavelength dependence of *S*. The Ångström exponent from this study (1.49±0.16) is within a reasonable range compared to previous studies. For example, the Ångström exponent was measured by a Raman lidar to be between 1.35±0.2 and 1.56±0.2 at 355 nm for smoke aerosols in Canada (Strawbridge et al., 2018). The Ångström exponent for urban aerosols was measured to be 1.4±0.5 in Europe and 1.7±0.5 in North America for 355 and 532 -nm ~~wavelengths~~ (Müller et al., 2007).

The Aerosol Robotic Network (AERONET) (Holben et al., 1998) provides aerosol optical depth (AOD) measurements in eight spectral bands between 340 and 1020 nm with a temporal resolution of about 15 min. The measurement uncertainty for AERONET AOD is within 0.02 and is expected to be larger in the UV bands (Eck et al., 1999; Holben et al., 2001). Even though the measurement is at a different wavelength, the AERONET AOD at 340 nm can provide an additional constraint for the choice of *S* for the RO_3QET aerosol retrieval, especially since both instruments are at the same location. Figure 2 presents the intercomparison of the RO_3QET lidar derived AOD at 299

Formatted: Font: Italic

Formatted: Font: Italic

nm and all available AOD data at 340 nm (Smirnov et al., 2000) from the collocated AERONET sun-sky radiometer (data for 21–23 June is unavailable). The near surface region is assumed to be homogeneous and assigned the same aerosol extinction values as the lowest available 30-m layer from the RO_3QET retrievals. Then, the aerosol extinction coefficients are integrated from 0 to 6 km asl to calculate the lidar-derived AOD. The omission of aerosol extinction above 6 km and the homogeneity assumption for the near surface region are sources of bias for the comparison since the AERONET instrument measures the total column AOD. The lidar has more data and higher temporal resolution, therefore, the lidar-derived AOD is interpolated to the AERONET measurement times. Figure 2 shows that the AOD retrieved by the two instruments has a correlation coefficient of 0.97 and a small RMSE for a total duration of about 31 hours. The mean percentage difference between the RO_3QET and AERONET AOD is 15±9%. The *S a priori* directly affects the AOD calculation. The lidar-derived AOD is on average 15% larger than the AERONET AOD due to the shorter wavelength of the lidar measurement suggesting that the choice of S = 60 sr is appropriate. For a rough estimation, the 1-σ standard deviation (9%) of the differences can be considered as the uncertainty of S if the variability of these differences are mostly due to the variation in S. Considering that AERONET measures the column average AOD, with longer temporal integration, has its own uncertainty, and covers only 38% of the total observational period, our assumption for S = 60 ±20% sr is appropriate for RO_3QET lidar profiling measurements with higher temporal and vertical resolution and should be good enough to cover various uncertainty sources. The collocated AERONET data enhances the credibility of our lidar aerosol retrieval and help evaluate the *S a priori*, with the caveat that the 124 paired data covering 31 hours is not a large sample. We do not show HSRL-AERONET comparison here since Reid et al. (2017) has done so using more extensive data in a visible band taken at the UAH site in summer 2013.

Figure 32 presents the intercomparison of the aerosol backscatter retrieved by the HSRL and the RO_3QET lidar for the four cases in 2013. The HSRL-derived aerosol backscatter coefficients are scaled to 299 nm (represented by "HSRL-converted" thereafter) using the best-fit exponent value $å_\beta$=1.34. Some clouds lower than 2 km show up in the HSRL curtains but not in the RO_3QET curtains (e. g., 1500–2100 on 15 August and 1500–2100 on 28 August). These low-cloud-contaminated data were discarded in the RO_3QET lidar pre-processing program since the ozone lidar probes the atmosphere with a shorter wavelength than the HSRL, and is therefore more affected by cloud interferencebecause the retrievable range was not long enough. The pProfiles with clouds higher than 2 km measured by the RO_3QET were retained and the aerosol retrievals below the clouds were used for the range-resolving intercomparisons.

In terms of the aerosol measurement evaluation, we pay attention to the two capabilities of the RO_3QET lidar's two capabilities: measuring the PBL diurnal evolution and measuring free-tropospheric smoke layers. In Figure 32, the PBL heights measured by the two lidars, which are identified by large aerosol gradients, are highly consistent for all cases. The development of the convective mixing layer in the early morning, an important process responsible for surface ozone increase, can be visually identified in most RO_3QET curtains (e.g., 1400–1700 UTC or 0900–1200 local time in Figure 32-h). The aerosol structures and evolutions in the free troposphere measured by the RO_3QET lidar are highly similar to those measured by the HSRL. For example, the RO_3QET lidar captured an extremely thin aerosol layer at ~5 km altitude on 27–28 August (Figure 32-g), which probably originated from the Pacific Northwest fire and has been discussed by Reid et al. (2017). The large aerosol uncertainties for the RO_3QET lidar at far ranges

Formatted: Font: Italic

Formatted: Font: Italic

Formatted: Font: Italic

are consistent with expectation. As demonstrated in Appendix B, aerosol retrieval uncertainties due to lidar signal measurement error and the boundary value chosen at the reference altitude, two of the most important sources of uncertainty, increase with altitude and may exceed 100% at ~7 km.

To evaluate the ~~ozone lidar's~~ range-resolving capability of the ozone lidar for aerosol retrieval, we intercompared the aerosol backscatter coefficients, for all cases, from the two instruments with a 10-min temporal resolution and a 30-m vertical resolution after filtering out cloud-contaminated data, as shown in Figure 4~~3~~. The high correlation coefficient of 0.95 suggests that the RO_3QET lidar can capture the aerosol variability with high spatio-temporal resolution~~s~~. The correlation coefficient (0.95) ~~for~~ between the two high vertical resolution retrievals is slightly lower~~less~~ than that between the RO_3QET and ~~for the~~ column–averaged HSRL retrievals (0.99, see ~~in~~ Figure 1) due to less vertical average ~~with respect to range~~. The HSRL-converted backscatter is calculated using $å_\beta$=1.34 and the regression equation in Figure 1. We expect the slope of the data in Figure 4 to be very close to 1. However, the actual slope is 1.08, reflecting the fact that there is a large fraction of points with small aerosol backscatter and larger residuals in clean air (low aerosol) regions. This is not surprising since the HSRL has higher measurement precision than the RO_3QET lidar so that their relative differences in clean air regions can be large.

Figure 5~~4~~ presents the mean and 1-σ standard deviations of the relative differences between RO_3QET and HSRL retrievals, (RO_3QET-HSRL)/HSRL, to be compared with the theoretical 1-σ error calculated as outlined in Appendix B. The HSRL measurements are considered as the "true" values to be compared with the RO_3QET measurements. Both the theoretical and actual 1-σ values generally increase with altitude. The actual differences between RO_3QET and HSRL measurements are mostly within or of comparable order of magnitude to the theoretical calculation of the RO_3QET measurement uncertainties. The structures of the theoretical uncertainties are consistent with the actual differences at most altitudes, with few exceptions. For example, the large discrepancies (red lines compared to blue lines in Figure 5~~4~~) occurring at ~4.5 km in Figure 5~~4~~ (c) and ~1.5 km in Figure 5~~4~~ (d) are primarily because of small number division effects for the extremely clean atmospheric layers (also see Figure 3~~2~~). Aerosol backscatter of clean air ~~probably~~ can be accurately measured by the HSRL, but~~,~~ may be beyond the measurement sensitivity of RO_3QET.

In Figure 5~~4~~, the RO_3QET-measured aerosols are generally higher than the HSRL-measured aerosols between 5 and 6 km so that the RO_3QET-HSRL differences ~~deflect~~ are biased to ~~the right side with altitude~~positive altitude values. These positive biases can be caused by two reasons. First, the RO_3QET derived aerosol extinction above 5 km is obviously larger than that from HSRL during daytime due to the solar background impact, which is especially strong in the summer. The relative differences are even worse in clean (compared to turbid) regions during the daytime because of the small number division effect mentioned earlier. It can be seen from Figure 3 that RO_3QET nighttime retrievals above 5 km and daytime retrievals below 5 km are relatively good due to either lower solar background or larger lidar signal resulting in better SNR. There were both clean ~~air~~ and smok~~y~~e layers between 5 and 6 km for the four cases; therefore, the positive differences cannot be explained solely by the lower capability of RO_3QET for measuring clean air. We hypothesize that another reason causing ~~these~~ the positive differences between 5 and 6 km is the underestimated backscatter color ratio for the smoke aerosols. We converted the HSRL backscatter from 532 to 299 nm using a constant backscatter color ratio, 1.34, which represents an average for the column-

integrated backscatter. The most ~~considerable~~ significant contribution to integrated backscatter comes from PBL aerosols, which are mostly urban aerosols with a lower backscatter color ratio than either fresh or aged smoke (Burton et al., 2012; Cattrall et al., 2005). The uncertainty of the backscatter color ratio was not considered in the error budget of the aerosol retrieval. In addition, we ignored the measurement uncertainty of the HSRL. Therefore, the general agreement of ~~the~~ theoretical estimates of ~~the~~ aerosol retrieval uncertainties and the actual errors suggests that our analysis of the uncertainty sources in Appendix B is reasonable.

4. Conclusions

We have evaluated the aerosol retrievals at 299 nm from the RO_3QET ozone lidar using both aerosol retrievals at 532 nm from the ~~highly precise~~ University of Wisconsin HSRL and AERONET AOD data at 340 nm from ~~the~~ coincident observations at Huntsville, AL in 2013. The integrated backscatter coefficients ~~between 0.4 and~~below 6 km asl ~~(0.2 and 5.8 km agl)~~ from ~~the two instruments~~RO_3QET and HSRL are highly correlated, with a Pearson coefficient of 0.99 after excluding cloud-contaminated data. ~~Since the ozone lidar is not able to accurately measure either ozone or aerosol above clouds, cloud-contaminated data can significantly distort the relationship between the products from the two instruments.~~ The aerosol profiles of backscatter coefficients at 30-m vertical and 10-min temporal resolution retrieved by ~~the~~ RO_3QET are also highly correlated with those from the HSRL with a coefficient of 0.95 suggesting that the ozone lidar is capable of ~~producing~~ providing reliable aerosol structure information at high spatio-temporal resolution. Intercomparison of the backscatter product was ~~chosen~~ performed to avoid additional uncertainty caused by the lidar ratio (S) assumption needed for the HSRL aerosol extinction retrieval. The RO_3QET-measured AOD below 6 km asl is also highly correlated with the AERONET-measured AOD, with a correlation coefficient of 0.97. The 340-nm band of the AERONET AOD data is closest to the ozone lidar wavelength among the available instruments and can therefore provide a constraint for the S assumption for the ozone lidar. Analysis of the intercomparison of AERONET and RO_3QET data confirms that our choice of S = 60 sr at 299 nm is appropriate.

The aerosol retrieval algorithm and its error budget are shown in the Appendix. The primary uncertainty sources for the aerosol lidar retrieval are errors in lidar signal measurement, boundary value assumption, air density calculation, *S a priori*, and ozone profile input. The uncertainty in S assumption is a dominant source at near range while the lidar signal measurement and boundary value errors dominate at far range, as shown in Figure B1 for a~~n example~~sample scenario. Within the middle range (PBL top – about 7 km), the air density calculation error is essential and is larger or comparable to the lidar signal measurement error. The total uncertainty generally increases with altitude from about 15% in the PBL to consistently higher than 100% above 7 km. Theoretical estimates of the error budget are generally consistent with ~~the~~ RO_3QET-HSRL measurement differences.

By assuming a constant S of 60 sr ~~for the ozone lidar~~at 299 nm, the backscatter coefficients measured by ~~the two instruments~~RO_3QET and HSRL are related by a backscatter color ratio (backscatter-related exponent) of 1.34±0.11 for 299 and 532 nm. The extinction-related Ångström exponent, that is more relevant for various applications, is estimated to be 1.49±0.16 by assuming S = 55 sr for the HSRL at 532 nm. These exponents represent a summertime average for a mixture of urban pollution and fire smoke. ~~We did not separate~~Separation of ~~the~~ aerosol types was not done in this work, although we ~~understand~~ recognize that S and Ångström exponent vary with the aerosol

Formatted: Font: Italic

phase function and size distribution. ~~The a~~Aerosol correction ~~in the~~for ozone lidar retrievals will be described in a subsequent paper.

Appendix A. Aerosol retrieval algorithm

The ozone DIAL solution can be written as follows:

$$n_{(r)} = \frac{-1}{2\Delta\sigma} \times \frac{d}{dr}\left[ln\frac{P_{\mathrm{on}(r)}}{P_{\mathrm{off}(r)}}\right] + [B] + [E]\,, \quad \text{(A1)}$$

where $n_{(r)}$ is the ozone number density at range r, $\Delta\sigma$ is the differential ozone absorption cross section, $P_{\mathrm{on}(r)}$ and $P_{\mathrm{off}(r)}$ are the backscattered on-line and off-line lidar returns, and $[B]$ and $[E]$ represent the differential backscatter and extinction terms (Browell et al., 1985), respectively, including both molecular and aerosol components. The first term of the right side of Eq. (A1) is often called the signal term. The subscripts "on" and "off" represent 289 and 299 nm ~~in~~for this study. The aerosol extinction coefficients at 299 nm are calculated using the following procedure.

1) A first-order Savitzky-Golay differentiation filter with a second-degree polynomial and variable fitting window widths are applied on $ln\frac{P_{\mathrm{on}(r)}}{P_{\mathrm{off}(r)}}$ to compute the signal term. This smoothing method can accommodate the rapid decay of the lidar signal with altitude to provide sufficient SNR for ozone retrievals by appropriate selection of smoothing window widths (Leblanc et al., 2016a).

2) By canceling the lidar constant using the two lidar equations at range r and $r+\Delta r$ for 299 nm, the aerosol backscatter coefficients at range r can be expressed as (Uchino et al., 1980):

$$\beta_A(r) = -\beta_M(r) + \frac{Z(r)}{Z(r+\Delta r)}[\beta_A(r+\Delta r) + \beta_M(r+\Delta r)]\exp\left\{-2\Delta r[\alpha_A\left(r+\frac{\Delta r}{2}\right) + \alpha_M\left(r+\frac{\Delta r}{2}\right) + \alpha_{O3}\left(r+\frac{\Delta r}{2}\right)]\right\}\,, \quad \text{(A2)}$$

where $\beta_A(r)$ and $\beta_M(r)$ are aerosol and molecular backscatter coefficients at range r, respectively; $Z(r) = P_{\mathrm{off}}r^2$ is the range-corrected lidar signal at 299 nm; $\alpha_A(r+\Delta r/2)$, $\alpha_M(r+\Delta r/2)$, and $\alpha_{O3}(r+\Delta r/2)$ represent the average aerosol, molecular, and ozone extinction coefficients between range r and $r+\Delta r$, respectively. Assuming the 299-nm lidar ratio, $S=\alpha_A/\beta_A$, is constant with the range at 60 sr for this study and further assuming:

$$\alpha_A(r+\tfrac{\Delta r}{2}) \approx \alpha_A(r+\Delta r) = S\beta_A(r+\Delta r), \quad \text{(A3)}$$

Eq. (A2) contains only two unknown variables: the aerosol backscatter coefficient $\beta_A(r+\Delta r)$ and ozone extinction coefficient $\alpha_{O3}(r+\Delta r/2)$, which requires knowledge of the ozone number density $n_{(r+\Delta r/2)}$. Molecular backscatter and extinction can be computed from nearby radiosonde data or a model with acceptable accuracy. For the first iteration step, $n_{(r+\Delta r/2)}$ can be computed from the signal term in Eq. (A1). By assuming a start value $\beta_A(\mathrm{ref})$ at a reference range and a constant S with range, $\beta_A(r)$ can be solved by Equation (A2). Then, the first $\beta_A(r)$ profile is substituted back into (A2) to compute the second estimate by using a more accurate form for $\alpha_A(r+\Delta r/2)$ as:

$$\alpha_A\left(r+\frac{\Delta r}{2}\right) = S[\beta_A(r+\Delta r) + \beta'_A(r)]/2, \quad \text{(A4)}$$

where $\beta'_A(r)$ represents the value from the first estimate. Typically, a stable solution for $\beta_A(r)$, which does not change significantly from one iteration step to the next, can be obtained with only three iterations of Eq. (A2) and (A4.

3) The correction terms, [B] and [E], in Eq. (A1) are calculated by the Browell et al. (1985) approximation, assuming a power law dependence with wavelength for the aerosol extinction and choosing an appropriate Ångström exponent. Since this paper focuses only on aerosol retrievals, the details of the ozone corrections will be described in a future article.

4) Aerosol profiles computed for the three altitude channels are finally merged to a single profile in their overlapping altitude zones, 0.5–1 km for Channels 1 and 2, 1.5–2 km for Channels 2 and 3.

Appendix B. Error budget of the aerosol retrieval

Now we investigate five primary error sources affecting each term on the right side of Eq. (A2). In the following section, we use the notation Δ to represent the absolute uncertainty and δ to represent the relative uncertainty. For a function Y, derived from several measurement variables x_1, x_2, …, the uncertainty in Y can be estimated by the following expression using the first-order Taylor expansion approximation when these variables are independent (Taylor, 1997):

$$\Delta Y^2 = (\Delta x_1 \frac{\partial Y}{\partial x_1})^2 + (\Delta x_2 \frac{\partial Y}{\partial x_2})^2 + \cdots . \quad \text{(B1)}$$

B.1 Lidar signal measurement error

The error source to determine the normalized lidar signal ratio term $\frac{Z(r)}{Z(r+\Delta r)}$ is the lidar signal measurement error, ΔP. Although ΔP may be due to various processes such as inaccurate dead-time correction, inaccurate background subtraction, and signal-induced noise, its dominant component is the lidar signal statistical uncertainty (often called lidar signal detection noise) and is typically assumed to obey a Poisson distribution. Assuming no error in deciding r, by using Eq. (A2) and (B1) we obtain the uncertainty of the aerosol backscatter owing to lidar signal measurement error, $\Delta\beta_A^{sig}(r)$, relative to the total backscatter as:

$$\frac{\Delta\beta_A^{sig}(r)}{\beta_A(r)+\beta_M(r)} = \sqrt{[\delta P(r)]^2 + [\delta P(r+\Delta r)]^2}, \quad \text{(B2)}$$

where $P(r)$ represents lidar signal counts at r after omitting the wavelength subscript (i.e., 299 nm) and $\delta P(r)$ is just the inverse of SNR. This means that the uncertainty of the aerosol backscatter coefficient due to lidar signal measurement is determined by the lidar SNR similarly to other remote sensing detection techniques. Consequently, its relative uncertainty can be written as:

$$\delta\beta_A^{sig}(r) = \left(\frac{1}{B(r)} + 1\right)\sqrt{[\delta P(r)]^2 + [\delta P(r+\Delta r)]^2}, \quad \text{(B3)}$$

where $B(r) = \beta_A(r)/\beta_M(r)$ is the aerosol-to-molecular backscatter ratio. As expected, $\delta\beta_A^{sig}(r)$ has a reverse relationship with $\beta_A(r)$ since it is a relative uncertainty. Figure B1 shows an example of the uncertainty budget for a 10-min lidar data profile. The aerosol retrieval uncertainty due to the lidar signal measurement error generally increases with altitude primarily because of the rapidly decaying lidar SNR.

B.2 Boundary value error

According to Eq. (A2), the uncertainty of the aerosol backscatter at r, $\beta_A(r)$, can be induced by the uncertainty of the backscatter at $r + \Delta r$, $\beta_A(r + \Delta r)$, due to the iterative computation method. The error propagation between the adjacent altitudes can be determined by their partial differential relationship. Using the traditional far-end solution by

assuming that the air is clean at a reference altitude, the aerosol uncertainty due to the inaccurate boundary value assumption propagates downward based on the following equation:

$$\delta\beta_A^{BV}(r) = \delta\beta_A(r+\Delta r)\left[\frac{1+\frac{1}{B(r)}}{1+\frac{1}{B(r+\Delta r)}}\right]\{1-2S\Delta r\beta_A(r+\Delta r)[1+\frac{1}{B(r+\Delta r)}]\}. \quad \text{(B4)}$$

The yellow line in Figure B1 represents the relative uncertainty of backscatter retrieval due to the boundary value assumption, $\delta\beta_A^{BV}(r)$, when $\delta\beta_A(r_b) = 1000\%$ (i.e., 10 times overestimate at r_b =10 km). Despite a large overestimate at the reference altitude, $\delta\beta_A^{BV}(r)$ decreases toward the ground, to less than 10% below 5.5 km and less than 1% below 3.5 km. Simulations demonstrate that $\delta\beta_A^{BV}(r)$ for an underestimation of $\delta\beta_A(r_b)$ (not shown) is better than that for an overestimation, indicating that the boundary value is preferred at a smaller value. As suggested by Eq. (B4), $\delta\beta_A^{BV}(r)$ is affected by both *S* and *B*. Larger *S* (if it is correct) results in smaller $\delta\beta_A^{BV}(r)$ and, therefore, aerosol retrieval errors converge to zero faster. In other words, the smaller the value of *S* is, the more sensitive the aerosol retrieval is to the boundary value error. $\delta\beta_A^{BV}(r)$ decreases with an increase of $B(r)$. This means that $\delta\beta_A^{BV}(r)$ is less affected by the assumed value of $\beta_A(r_b)$ when the aerosol backscatter becomes more important relative to molecular backscatter, which occurs at longer wavelengths or under turbid air conditions. It is to be noted that $\delta\beta_A(r_b)$ is between -1 and $+\infty$ so that the distribution of $\delta\beta_A^{BV}(r)$ is asymmetric with the zero axis.

In terms of the influence of the boundary value error, we have compared our calculation with an analytical solution proposed by Kovalev and Moosmüller (1994) (not shown); the results are almost identical. Aerosol retrieval uncertainty due to incorrect boundary value assumption tends to converge to zero towards the lidar. It is negligible at lower altitudes, especially in the PBL, when the air is turbid.

B.3 Air density error

According to Eq. (A2), the air density profile affects $\beta_M(r)$, $\beta_M(r+\Delta r)$, and the optical depth (or transmittance). Similarly, we can derive the relative uncertainty in aerosol backscatter owing to the uncertainty in the air density profile as:

$$\delta\beta_A^{AD}(r) = \sqrt{\{\frac{\delta\beta_M(r)}{B(r)}[1+S_m\Delta r\beta_A(r)+S_m\Delta r\beta_M(r)]\}^2+\{\frac{\delta\beta_M(r+\Delta r)\left[\frac{1}{B(r)}+1\right]}{B(r+\Delta r)+1}[1-S_m\Delta r\beta_A(r+\Delta r)-S_m\Delta r\beta_M(r+\Delta r)]\}^2}$$

. (B5)

S_m represents the molecular extinction-to-backscatter ratio, which is a constant ($8\pi/3$). The two parts in the square root are the components due to the uncertainties at r and $r+\Delta r$, respectively. Each component includes the influences from both molecular backscatter and optical depth. When Δr is small, the contribution of the optical depth error is much smaller than that of the molecular backscatter error so that (B4) can be approximated as:

$$\delta\beta_A^{AD}(r) \approx \sqrt{2}\frac{\delta\beta_M(r)}{B(r)}. \quad \text{(B6)}$$

It is to be noted that $\Delta\beta_M(r)$ and $\Delta\beta_M(r+\Delta r)$ are independent errors as assumed in Eq. (B1). If they are correlated, Eq. (B5) will partly cancel out with their covariance term, which is not shown in (B1). Due to the nature of the iterative computation method, $\delta\beta_A^{AD}(r+\Delta r)$ affects $\delta\beta_A^{AD}(r)$ as noted in Eq. (B4), so that the aerosol retrieval uncertainty due to air density error will propagate downward. However, model simulation suggests that the systematic error of the air

density calculation has little impact on the aerosol retrieval because of the cancelation of the effect at r and $r + \Delta r$. Eq. (B6) means the uncertainty in the calculation of molecular backscatter will mostly linearly propagate to aerosol backscatter. If the 2-σ precision of a radiosonde is 0.3 K and 0.5 hPa for temperature and pressure measurements (Hurst et al., 2011), the propagated uncertainty onto molecular backscatter is only about 0.1%. However, the real disturbance of an atmosphere deviating from the actual air density profile may be more significant since there are usually only a few radiosonde profiles available every day. Hence, we assume $\delta\beta_M(r)$ to be 1% and the resulting aerosol retrieval uncertainty is represented by the green line in Figure B1. $\delta\beta_A^{AD}(r)$ can be tens of percent in the free troposphere and is an important error source for aerosol retrievals (Russell et al., 1979). $\delta\beta_A^{AD}(r)$ is less than 10% in the PBL because of more turbid air in that region. Since $\delta\beta_M(r)$ is assumed to be a constant in this example, the variation of $\delta\beta_A^{AD}(r)$ is mostly a result of varying $B(r)$, the aerosol-to-molecular backscatter ratio. Since $B(r)$ generally increases with an increase in wavelength, $\delta\beta_A^{AD}(r)$ is expected to be smaller at longer wavelengths. Therefore, the aerosol retrieval is less sensitive to the air density error at longer wavelengths.

B.4 Lidar ratio error

By using Eqn. (A2) and (B1), the relative uncertainty in aerosol backscatter due to incorrect lidar ratio (S) assumption can be calculated as follows:

$$\delta\beta_A^S(r) = 2\left[\frac{1}{B(r)} + 1\right]\Delta S\beta_A(r)\Delta r. \quad \text{(B7)}$$

$\delta\beta_A^S(r)$ due to ΔS at only range r appears to be small, about 1%, when Δr is specified at 22.5 m. However, ΔS varying with altitude is mostly systematic and, therefore, $\delta\beta_A^S(r)$ at every altitude will propagate downward and these effects will accumulate. The error accumulation is not straightforward to compute as an analytical solution. However, these effects can be simulated numerically. S is highly variable and it is difficult to estimate its actual uncertainty range. In this study, we assume that $\delta S = 20\%$ (or ΔS =12 sr) according to ~~a~~ both previous study (Müller et al., 2007) and the analysis using the collocated AERONET AOD data at 340 nm. The light-blue line in Figure B1 shows that the accumulative uncertainties in the aerosol backscatter due to ΔS using Eq. (B7) and (B4) are close to the assumed 20% uncertainty for δS. $\delta\beta_A^S(r)$ is the largest error source in the PBL which is the near range of the lidar. $\delta\beta_A^S(r)$ decreases with an increase in wavelength because of increasing $B(r)$. In other words, $\delta\beta_A^S(r)$ is less sensitive to ΔS at longer wavelengths.

B.5 Ozone error

Similar to S, the ozone uncertainty affects only the transmittance term in Eqn. (A2) and its error propagation on aerosol backscatter retrieval can be expressed as:

$$\delta\beta_A^{O3}(r) = 2\left[\frac{1}{B(r)} + 1\right]\Delta\alpha_{O3}(r)\Delta r. \quad \text{(B8)}$$

$\delta\beta_A^{O3}(r)$ is proportional to the $\left[\frac{1}{B(r)} + 1\right]$ factor and ozone absorption uncertainty, meaning that $\delta\beta_A^{O3}(r)$ is smaller at longer wavelengths due to larger aerosol scattering ratio and smaller ozone absorption. When Δr is specified at 22.5 m, $\delta\beta_A^{O3}(r)$ is less than 0.3%. We still simulate the vertical accumulation of $\delta\beta_A^{O3}(r)$ using Eq. (B4). As noted earlier, the systematic errors of the DIAL ozone measurement tend to accumulate while the random errors tend to cancel out. The dominant error source for lidar measurements at the far range is typically the lidar signal detection noise, a type

of random error. Therefore, for purposes of estimation, we assume a 5% constant DIAL retrieval uncertainty primarily covering the uncertainties due to ozone absorption cross section, non-ozone gas interference, and signal saturation effect (Leblanc et al., 2018; Wang et al., 2017). As shown in Figure B1, the simulated aerosol retrieval uncertainty due to ozone is relatively minor and is less than 5% at most altitudes.

In summary, the uncertainties in aerosol backscatter retrieval for the ozone lidar are controlled by ΔS at near ranges (i. e., in the PBL) where the air is most turbid and are determined by both the lidar signal detection error and inaccurate boundary value assumption at far ranges (higher than 7 km) where the air is typically clear. In the middle range of the lidar measurement (PBL top – 7 km), the air density calculation error may become a significant error source for aerosol retrieval and may have a comparable influence on the aerosol retrieval as the lidar signal measurement error. Relative to the above four uncertainty sources, ozone DIAL retrieval error is relatively unimportant especially in the lower altitudes where lidar SNR is large enough. All the uncertainty terms are affected by the aerosol-to-molecular backscatter ratio, $B(r)$, which represents the relative importance of the aerosol component in both extinction and backscatter processes. Based on the above uncertainty budget analysis, we conclude that the RO_3QET lidar is capable of measuring aerosol profile reliably below 6 km with the current laser output power.

Acknowledgements

The authors thank the National Aeronautics and Space Administration (NASA)'s Science Mission Directorate for supporting the TOLNet program. A portion of the research was carried out at the Jet Propulsion Laboratory, California Institute of Technology, under a contract with the National Aeronautics and Space Administration (80NM0018D0004). The views, opinions, and findings contained in this report are those of the authors and should not be construed as an official NASA, National Oceanic and Atmospheric Administration, or U.S. Government position, policy, or decision.

References

Ackermann, J. (1998). The extinction-to-backscatter ratio of tropospheric aerosol: A numerical study. *Journal of atmospheric and oceanic technology*, *15*(4), 1043-1050.

Alvarez, R. J., Senff, C. J., Langford, A. O., Weickmann, A. M., Law, D. C., Machol, J. L., ... & Hardesty, R. M. (2011). Development and application of a compact, tunable, solid-state airborne ozone lidar system for boundary layer profiling. *Journal of Atmospheric and Oceanic Technology*, *28*(10), 1258-1272.

Ångström, A. (1929). On the atmospheric transmission of sun radiation and on dust in the air. *Geografiska Annaler*, *11*(2), 156-166.

Browell, E. V., Ismail, S., and Shipley, S. T. (1985)~~:~~. Ultraviolet DIAL measurements of O3 profiles in regions of spatially inhomogeneous aerosols, Appl. Opt., 24(17), 2827-2836~~, 1985~~.

Browell, E. V., Fenn, M. A., Butler, C. F., Grant, W. B., Harriss, R. C., & Shipham, M. C. (1994). Ozone and aerosol distributions in the summertime troposphere over Canada. *Journal of Geophysical Research: Atmospheres*, *99*(D1), 1739-1755.

Burton, S. P., Ferrare, R. A., Hostetler, C. A., Hair, J. W., Rogers, R. R., Obland, M. D., ... & Froyd, K. D. (2012). Aerosol classification using airborne High Spectral Resolution Lidar measurements–methodology and examples. *Atmospheric Measurement Techniques*, *5*(1), 73-98.

Cattrall, C., Reagan, J., Thome, K., & Dubovik, O. (2005). Variability of aerosol and spectral lidar and backscatter and extinction ratios of key aerosol types derived from selected Aerosol Robotic Network locations. *Journal of Geophysical Research: Atmospheres*, *110*(D10).

De Young, R., Carrion, W., Ganoe, R., Pliutau, D., Gronoff, G., Berkoff, T., & Kuang, S. (2017). Langley mobile ozone lidar: ozone and aerosol atmospheric profiling for air quality research. *Applied optics*, *56*(3), 721-730.

Eck, T. F., Holben, B. N., Reid, J. S., Dubovik, O., Smirnov, A., O'neill, N. T., ... & Kinne, S. (1999). Wavelength dependence of the optical depth of biomass burning, urban, and desert dust aerosols. *Journal of Geophysical Research: Atmospheres*, *104*(D24), 31333-31349.

Eisele, H., & Trickl, T. (2005). Improvements of the aerosol algorithm in ozone lidar data processing by use of evolutionary strategies. *Applied optics*, *44*(13), 2638-2651.

Eloranta, E. E. (2005). High spectral resolution lidar. In *Lidar* (pp. 143-163). Springer, New York, NY.

Fernald, F. G. (1984). Analysis of atmospheric lidar observations: some comments. *Applied optics*, *23*(5), 652-653.

Fukuchi, T., Fujii, T., Cao, N., Nemoto, K., & Takeuchi, N. (2001). Tropospheric O3 measurement by simultaneous differential absorption lidar and null profiling and comparison with sonde measurement. *Optical Engineering*, *40*.

Gronoff, G., Robinson, J., Berkoff, T., Swap, R., Farris, B., Schroeder, J., ... & Adcock, E. E. (2019). A method for quantifying near range point source induced O3 titration events using Co-located Lidar and Pandora measurements. *Atmospheric Environment*, *204*, 43-52.

Grund, C. J., & Eloranta, E. W. (1991). University of Wisconsin high spectral resolution lidar. *Optical Engineering*, *30*(1), 6-13.

Groß, S., Esselborn, M., Weinzierl, B., Wirth, M., Fix, A., & Petzold, A. (2013). Aerosol classification by airborne high spectral resolution lidar observations. *Atmospheric chemistry and physics*, *13*(5), 2487-2505.

Hair, J. W., Hostetler, C. A., Cook, A. L., Harper, D. B., Ferrare, R. A., Mack, T. L., ... & Hovis, F. E. (2008). Airborne high spectral resolution lidar for profiling aerosol optical properties. *Applied optics*, *47*(36), 6734-6752.

Holben, B. N., Eck, T. F., Slutsker, I. A., Tanre, D., Buis, J. P., Setzer, A., ... & Lavenu, F. (1998). AERONET—A federated instrument network and data archive for aerosol characterization. *Remote sensing of environment*, *66*(1), 1-16.

Holben, B. N., Tanre, D., Smirnov, A., Eck, T. F., Slutsker, I., Abuhassan, N., ... & Kaufman, Y. J. (2001). An emerging ground-based aerosol climatology: Aerosol optical depth from AERONET. *Journal of Geophysical Research: Atmospheres*, *106*(D11), 12067-12097.

Hurst, D. F., Hall, E. G., Jordan, A. F., Miloshevich, L. M., Whiteman, D. N., Leblanc, T., ... & Oltmans, S. J. (2011). Comparisons of temperature, pressure and humidity measurements by balloon-borne radiosondes and frost point hygrometers during MOHAVE-2009. *Atmospheric Measurement Techniques*, *4*(12), 2777-2793.

Immler, F. (2003). A new algorithm for simultaneous ozone and aerosol retrieval from tropospheric DIAL measurements. *Applied Physics B*, *76*(5), 593-596.

Kempfer, U., Carnuth, W., Lotz, R., & Trickl, T. (1994). A wide-range ultraviolet lidar system for tropospheric ozone measurements: Development and application. *Review of scientific instruments*, *65*(10), 3145-3164.

Klein, A., Ravetta, F., Thomas, J. L., Ancellet, G., Augustin, P., Wilson, R., ... & Pelon, J. (2019). Influence of vertical mixing and nighttime transport on surface ozone variability in the morning in Paris and the surrounding region. *Atmospheric environment*, *197*, 92-102.

Klett, J. D. (1981). Stable analytical inversion solution for processing lidar returns. *Applied optics*, *20*(2), 211-220.

Klett, James D. "Lidar inversion with variable backscatter/extinction ratios." *Applied optics* 24.11 (1985): 1638-1643.

Kovalev, V. A., & Eichinger, W. E. (2004). *Elastic lidar: theory, practice, and analysis methods*. John Wiley & Sons.

Kovalev, V. A., & Moosmüller, H. (1994). Distortion of particulate extinction profiles measured with lidar in a two-component atmosphere. *Applied optics*, *33*(27), 6499-6507.

Kovalev, V. A., & McElroy, J. L. (1994). Differential absorption lidar measurement of vertical ozone profiles in the troposphere that contains aerosol layers with strong backscattering gradients: a simplified version. *Applied optics*, *33*(36), 8393-8401.

Kuang, S., Burris, J. F., Newchurch, M. J., Johnson, S., and Long, S.: Differential Absorption Lidar to Measure Subhourly Variation of Tropospheric Ozone Profiles, IEEE Transactions on Geoscience and Remote Sensing, 49, 557-571, 10.1109/TGRS.2010.2054834, 2011.

Kuang, S., Newchurch, M. J., Burris, J., and Liu, X.: Ground-based lidar for atmospheric boundary layer ozone measurements, Appl. Opt., 52, 3557-3566, 10.1364/AO.52.003557, 2013.

Kuang, S., Newchurch, M. J., Johnson, M. S., Wang, L., Burris, J., Pierce, R. B., ... & Warneke, C. (2017). Summertime tropospheric ozone enhancement associated with a cold front passage due to stratosphere-to-troposphere transport and biomass burning: Simultaneous ground-based lidar and airborne measurements. *Journal of Geophysical Research: Atmospheres*, *122*(2), 1293-1311.

Langford, A. O., Alvarez, I. I., Raul, J., Kirgis, G., Senff, C. J., Caputi, D., ... & McNamara, M. E. (2019). Intercomparison of lidar, aircraft, and surface ozone measurements in the San Joaquin Valley during the California Baseline Ozone Transport Study (CABOTS). *Atmospheric Measurement Techniques*, *12*(3), 1889-1904.

Langford, A. O., Alvarez, R. J., Brioude, J., Caputi, D., Conley, S. A., Evan, S., ... & Ryoo, J. M. (2020). Ozone production in the Soberanes smoke haze: implications for air quality in the San Joaquin Valley during the California Baseline Ozone Transport Study. *Journal of Geophysical Research: Atmospheres*, *125*(11), e2019JD031777.

Leblanc, T., Sica, R. J., van Gijsel, J. A. E., Godin-Beekmann, S., Haefele, A., Trickl, T., Payen, G., and Gabarrot, F.: Proposed standardized definitions for vertical resolution and uncertainty in the NDACC lidar ozone and temperature algorithms – Part 1: Vertical resolution, Atmos. Meas. Tech., 9, 4029-4049, 10.5194/amt-9-4029-2016, 2016a.

Leblanc, T., Sica, R.J., Van Gijsel, J.A., Godin-Beekmann, S., Haefele, A., Trickl, T., Payen, G. and Liberti, G., 2016. Proposed standardized definitions for vertical resolution and uncertainty in the NDACC lidar ozone and temperature algorithms–Part 2: Ozone DIAL uncertainty budget. Atmospheric Measurement Techniques, 9(8), pp.4051-4078, 2016b.

Leblanc, T., Brewer, M. A., Wang, P. S., & Granados Muñoz, M. J. (2018). Validation of the TOLNet lidars: the Southern California Ozone Observation Project (SCOOP). *Atmospheric measurement techniques*, *11*, 6137-6162.

McDermid, I. S., Beyerle, G., Haner, D. A., & Leblanc, T. (2002). Redesign and improved performance of the tropospheric ozone lidar at the Jet Propulsion Laboratory Table Mountain Facility. *Applied optics*, *41*(36), 7550-7555.

Mishchenko, M. I., Travis, L. D., Kahn, R. A., & West, R. A. (1997). Modeling phase functions for dustlike tropospheric aerosols using a shape mixture of randomly oriented polydisperse spheroids. *Journal of Geophysical Research: Atmospheres*, *102*(D14), 16831-16847.

Müller, D., Ansmann, A., Mattis, I., Tesche, M., Wandinger, U., Althausen, D., & Pisani, G. (2007). Aerosol-type-dependent lidar ratios observed with Raman lidar. *Journal of Geophysical Research: Atmospheres*, *112*(D16).

Newell, R. E., Thouret, V., Cho, J. Y., Stoller, P., Marenco, A., & Smit, H. G. (1999). Ubiquity of quasi-horizontal layers in the troposphere. *Nature*, *398*(6725), 316.

Papayannis, A. D., Porteneuve, J., Balis, D., Zerefos, C., & Galani, E. (1999). Design of a new DIAL system for tropospheric and lower stratospheric ozone monitoring in Northern Greece. *Physics and Chemistry of the Earth, Part C: Solar, Terrestrial & Planetary Science*, *24*(5), 439-442.

Proffitt, M. H., & Langford, A. O. (1997). Ground-based differential absorption lidar system for day or night measurements of ozone throughout the free troposphere. *Applied optics*, *36*(12), 2568-2585.

Reid, J. S., Kuehn, R. E., Holz, R. E., Eloranta, E. W., Kaku, K. C., Kuang, S., ... & Atwood, S. A. (2017). Ground-based High Spectral Resolution Lidar observation of aerosol vertical distribution in the summertime Southeast United States. *Journal of Geophysical Research: Atmospheres*, *122*(5), 2970-3004.

Russell, P. B., Swissler, T. J., & McCormick, M. P. (1979). Methodology for error analysis and simulation of lidar aerosol measurements. *Applied Optics*, *18*(22), 3783-3797.

Smirnov, A., Holben, B. N., Eck, T. F., Dubovik, O., & Slutsker, I. (2000). Cloud-screening and quality control algorithms for the AERONET database. *Remote sensing of environment*, *73*(3), 337-349.

Steinbrecht, W., & Carswell, A. I. (1995). Evaluation of the effects of Mount Pinatubo aerosol on differential absorption lidar measurements of stratospheric ozone. *Journal of Geophysical Research: Atmospheres*, *100*(D1), 1215-1233.

Strawbridge, K. B., Travis, M. S., Firanski, B. J., Brook, J. R., Staebler, R., & Leblanc, T. (2018). A fully autonomous ozone, aerosol and nighttime water vapor lidar: a synergistic approach to profiling the atmosphere in the Canadian oil sands region. *Atmospheric Measurement Techniques*, *11*(12), 6735-6759.

Sullivan, J. T., McGee, T. J., Sumnicht, G. K., Twigg, L. W., & Hoff, R. M. (2014). A mobile differential absorption lidar to measure sub-hourly fluctuation of tropospheric ozone profiles in the Baltimore–Washington, DC region. *Atmospheric Measurement Techniques*, *7*(10), 3529-3548.

Taylor, J. (1997). *Introduction to error analysis, the study of uncertainties in physical measurements*.

Uchino, O., Maeda, M., Shibata, T., Hirono, M., & Fujiwara, M. (1980). Measurement of stratospheric vertical ozone distribution with a Xe–Cl lidar; estimated influence of aerosols. *Applied optics*, *19*(24), 4175-4181.

Uchino, O., & Tabata, I. (1991). Mobile lidar for simultaneous measurements of ozone, aerosols, and temperature in the stratosphere. *Applied optics*, *30*(15), 2005-2012.

Wang, L., Newchurch, M. J., Alvarez II, R. J., Berkoff, T. A., Brown, S. S., Carrion, W., DeYoung R. J., Johnson, B. J., Ganoe, R., Gronoff, G., Kirgis G., Kuang, S., Langford, A. O., Leblanc T., McDuffie E. E., McGee, T. J., Pliutau, D., Senff, C. J., Sullivan, J. T., Sumnicht, G., Twigg, L. W., & Weinheimer, A. J. (2017). Quantifying TOLNet ozone lidar accuracy during the 2014 DISCOVER-AQ and FRAPPE campaigns. *Atmospheric Measurement Techniques*, 10(10), 3865-3876.

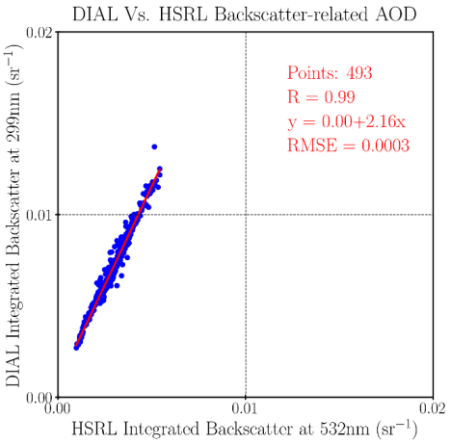

Figure 1. Regression of ~~the~~ ozone DIAL~~lidar~~ and HSRL derived integrated aerosol backscatter between 0.4 and 6 km asl using the best least-square~~s~~ fit, resulting in a backscatter color ratio of 1.34 for 299–532-nm for four cases in 2013. All the data was taken at Huntsville, AL, USA, during ~~the~~ summer~~time~~ 2013.

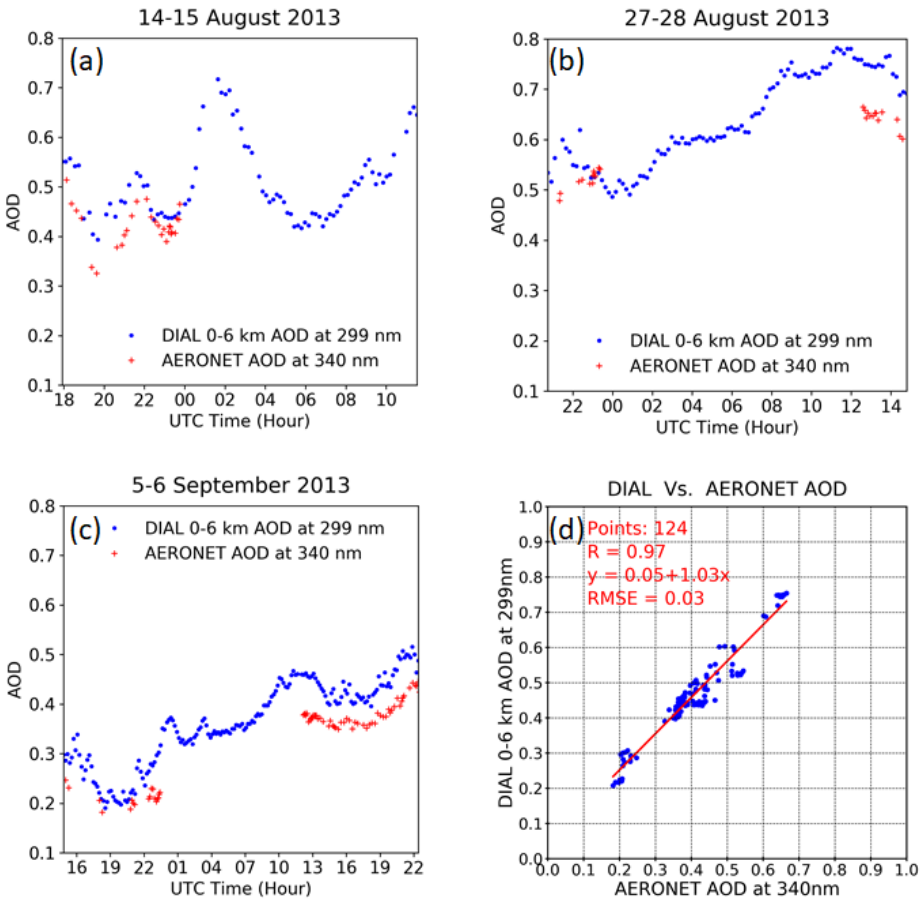

Figure 2. RO$_3$QET DIAL derived AOD between 0 and 6 km at 299 nm using S=60 sr compared to collocated AERONET AOD at 340 nm for (a) 14–15 August, (b) 27–28 August, and (c) 5–6 September, 2013. (d) Regression of the paired data after the DIAL AOD is interpolated to the times of AERONET AOD measurements.

Formatted: Centered

Formatted: Justified

Formatted: Subscript

Formatted: Font: Italic

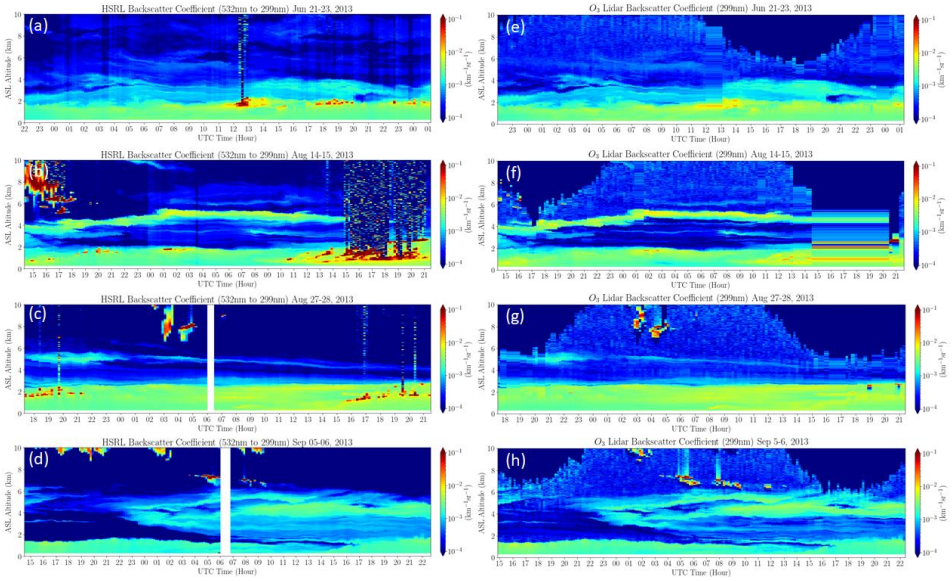

Figure 3~~2~~. HSRL-converted aerosol backscatter coefficients (a, b, c, d) compared to ~~the~~ RO_3QET lidar–derived aerosol backscatter coefficients at 299 nm (e, f, g, h), with 10-min temporal resolution and 30-m vertical resolution. The data was taken from 21–23 June (a, e), 14–15 August (b, f), 27–28 August (c, g), and 5–6 September (d, h) 2013. The HSRL-converted aerosol backscatter coefficients are scaled from the original retrievals at 532 nm to 299 nm using Eq. (1) and $å_\beta$=1.34.

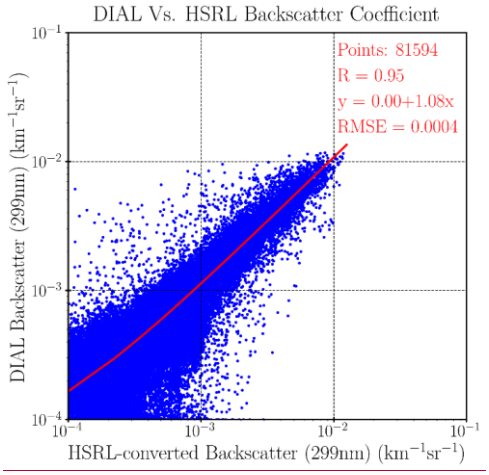

Figure 43. Regression of ~~the~~ ozone lidar measured and HSRL-converted aerosol backscatter coefficients (interpolated to~~at~~ 299 nm with $å_{\beta}$=1.34) with 30-m vertical resolution and 10-min temporal resolution. The regression line is a little curved in log scale because the intercept is not exactly zero.

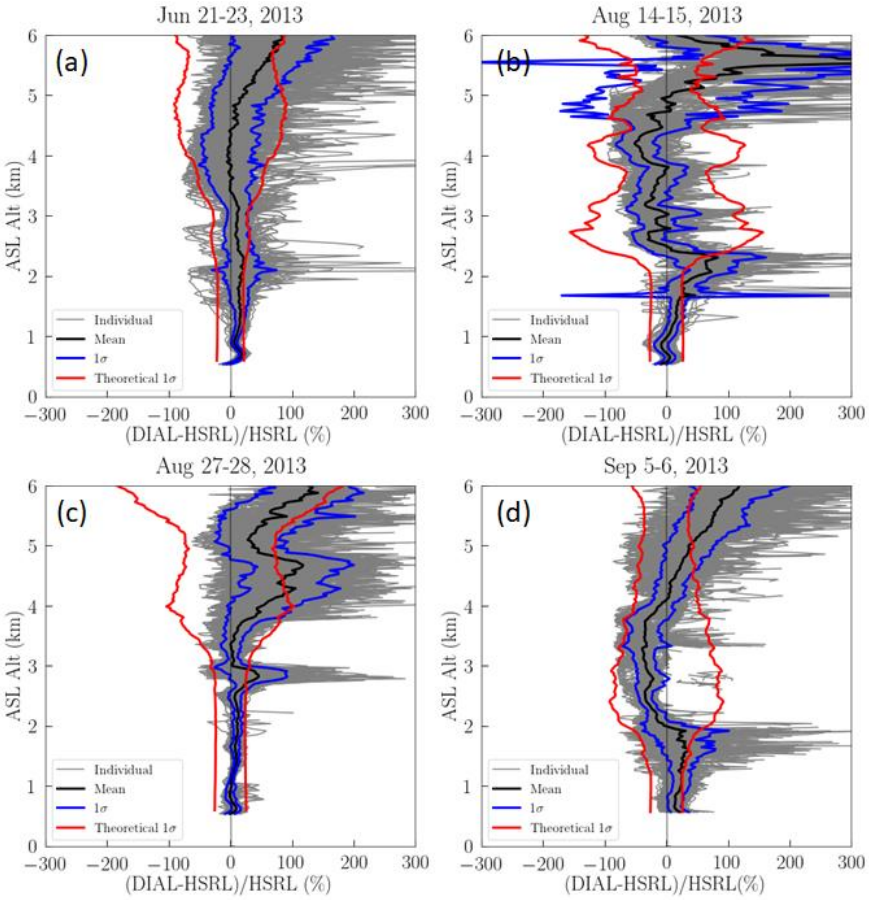

Figure 54. Relative differences between ~~the~~ RO_3QET and HSRL-converted aerosol backscatter measurements, (RO_3QET-HSRL)/HSRL, made from (a) 21–23 June, (b) 14–15 August, (c) 27–28 August, and (d) 5–6 September, 2013. The gray and black lines represent the differences for the10-min individual aerosol backscatter profiles and their mean, respectively. The blue lines represent the actual 1 σ of the differences compared to the theoretical 1 σ (red lines) of the RO_3QET lidar aerosol measurement.

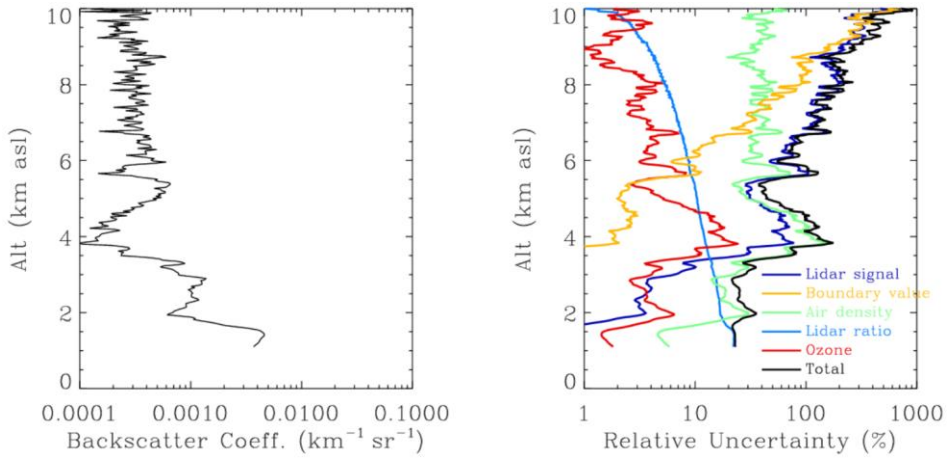

(a) (b)

Figure B1. An example of (a) aerosol backscatter profile retrieved from ~~a~~ 10-min ozone lidar data at about 8:30 UTC on 22 June 2013 and (b) ~~its~~ the retrieval error budget for different uncertainty sources. The lidar data was from the Channel-3 receiving system which covers most of the measurement altitude range and was arbitrarily chosen for a cloud-free ~~condition~~scenario.